



# Origin of compositional trends in clinopyroxene of oceanic gabbros and gabbroic rocks: A case study using data from ODP Hole 735B

Sofia Stone, Yaoling Niu\*

Department of Earth Sciences, Durham University, Durham DH1 3LE, UK

## ARTICLE INFO

### Article history:

Received 29 November 2008

Accepted 17 April 2009

Available online 3 May 2009

### Keywords:

ocean ridge magmatism  
oceanic lower crustal gabbros  
MORB differentiation  
mineral stoichiometry  
clinopyroxene compositional systematics

## ABSTRACT

The Ocean Drilling Program Hole 735B near the Southwest Indian Ridge represents the most complete *in situ* section of oceanic lower crust. The drill core samples are gabbros with several sub-divisions defined by varying amounts of minor phases. These samples have been subject to many studies. Among several yet to be understood phenomena is an apparently unexpected observation in the compositions of the constituent clinopyroxene (cpx).  $\text{TiO}_2$  and  $\text{Na}_2\text{O}$  in cpx do not show expected inverse correlations with  $\text{Mg}_{\text{Cpx}}^{\#}$ . Instead, both  $\text{TiO}_2$  and  $\text{Na}_2\text{O}$  increase with decreasing  $\text{Mg}_{\text{Cpx}}^{\#}$ , reaching a maximum at  $\text{Mg}_{\text{Cpx}}^{\#} = -0.76$ – $-0.73$ . With continued  $\text{Mg}_{\text{Cpx}}^{\#}$  decrease,  $\text{TiO}_2$  decreases sharply whereas  $\text{Na}_2\text{O}$  declines gently and flattens out. This observation has been previously interpreted as resulting from boundary layer crystallization within a steady-state magma chamber. In this study, we show that the  $\text{Na}_2\text{O}$ – $\text{Mg}_{\text{Cpx}}^{\#}$  and  $\text{TiO}_2$ – $\text{Mg}_{\text{Cpx}}^{\#}$  co-variations in cpx can be explained as a straightforward consequence of basaltic magma evolution and related cpx crystal stoichiometry control without invoking complex magma chamber processes. Our interpretation is superior to the boundary layer crystallization model (1) because the latter requires a steady-state magma chamber that is inconsistent with the observation of melt emplacement as thin sills, making convective and steady-state magma chambers unlikely at the slow-spreading Southwest Indian Ridge; and (2) because the  $\text{TiO}_2$  and  $\text{Na}_2\text{O}$  maxima in cpx correspond to the onset and continued crystallization of Fe–Ti oxides or the basalt–andesite transition stage of tholeiitic basaltic melt evolution.

© 2009 Elsevier B.V. All rights reserved.

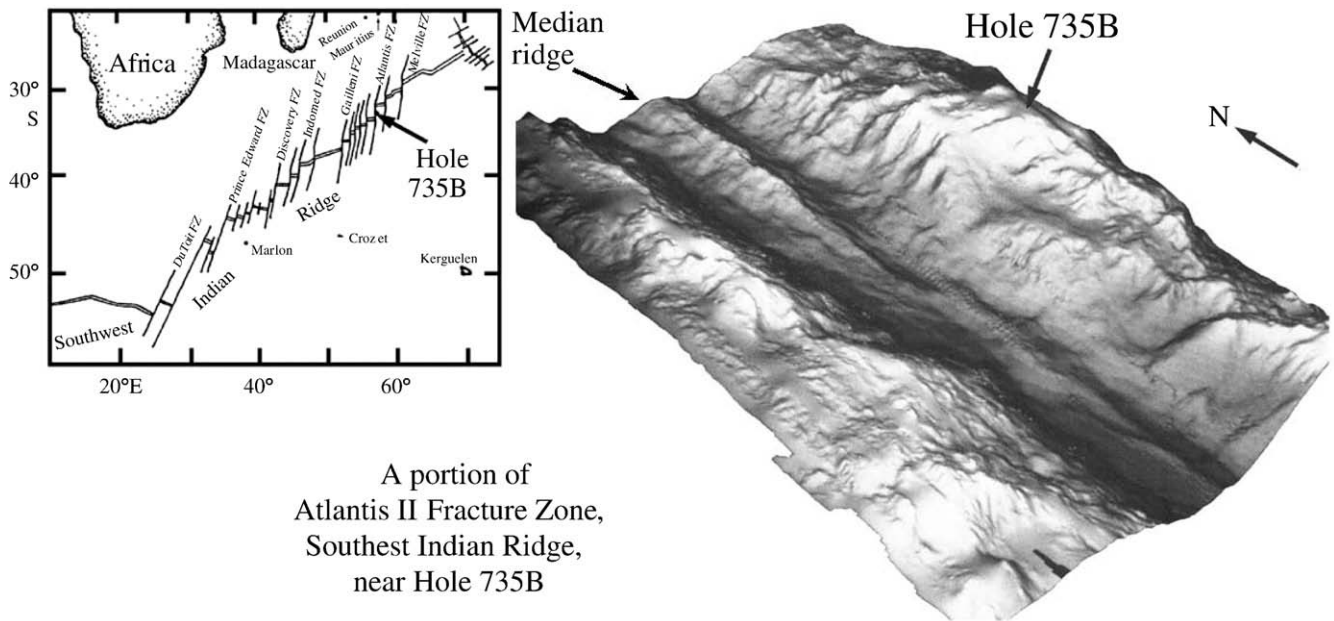
## 1. Introduction

Ocean ridge magmatism, which creates the ocean crust, has received much attention since the advent of plate tectonics theory ~40 years ago. The processes of magma generation and evolution at ocean ridges are generally thought to be much better understood than those in other major tectonic settings on Earth. However, many fundamental details remain poorly understood. For example, how melts produced in a broad region in the sub-ridge mantle migrate and focus towards the very narrow axial zone of crustal accretion remains enigmatic (e.g., Niu, 1997). It is well established experimentally that “primary” mantle melts must be in equilibrium with mantle mineralogy (e.g., O'Hara, 1968; Walker et al., 1979; Stolper, 1980), yet all the erupted MORB melts are much more evolved (e.g., Natland, 1980; Langmuir et al., 1992; Sinton and Detrick, 1992; Batiza and Niu, 1992). Cooling of mantle melts during ascent through the shallow mantle (Niu, 1997, 2004; Niu and Hékinian, 1997a,b) and within crustal level magma chambers (O'Hara, 1977; O'Hara and Mathews, 1981; Natland, 1980; Langmuir, 1989; Sinton and Detrick, 1992) must be the primary mechanism of melt evolution, but the concept and physical size of presumed/perceived ocean ridge magma chambers

have evolved over the years (e.g., Natland, 1980; Sinton and Detrick, 1992; Natland and Dick, 2001). As a result, physical processes of magma differentiation and ocean crust accretion are not so well understood as previously thought (e.g., Kelemen et al., 1997; MacLeod and Yaouancq, 2000; Dick et al., 2000, 2002). Conceptually, the oceanic lower crust gabbros represent fossil crustal magma chambers where mantle derived melts differentiate and evolve (e.g., Sinton and Detrick, 1992). However, detailed investigations have recognized that gabbros are exceedingly complex on all scales (Kelemen et al., 1997; Dick et al., 2000; MacLeod and Yaouancq, 2000; Coogan et al., 2000; Bach et al., 2001; Natland and Dick, 2001; Niu et al., 2002a; Coogan, 2007), making it necessary to reconsider models of magma chambers and processes of magma differentiation at crustal levels.

In this short contribution, we do not wish to resolve ocean ridge magma chamber problems, but to offer conceptually new interpretations to some well documented, yet thus far unsatisfactorily explained compositional systematics in the clinopyroxene (cpx; e.g.,  $\text{TiO}_2$  and  $\text{Na}_2\text{O}$ ) of oceanic lower crustal gabbroic lithologies, whose significance has been previously noted in drill core samples from the Atlantis Bank at the Southwest Indian Ridge (SWIR), i.e., ODP Holes 735B and 1105A (Dick et al., 2000, 2002; Natland and Dick, 2002; Niu et al., 2002a; Thy, 2003; Casey et al., 2007). Because the data set from Hole 735B is the largest and most coherent of its kind, we base our analysis and discussion on this data set. Among several findings, we demonstrate

\* Corresponding author. Tel.: +44 19 1334 2311; fax: +44 19 1334 2301.  
E-mail address: [Yaoling.Niu@durham.ac.uk](mailto:Yaoling.Niu@durham.ac.uk) (Y. Niu).



A portion of  
Atlantis II Fracture Zone,  
Southwest Indian Ridge,  
near Hole 735B

**Fig. 1.** Left, geological context of the Atlantis II transform at the slow-spreading Southwest Indian Ridge (SWIR). Right, satellite and gravity image of the Atlantis II transform and its eastern shoulder (Atlantis Bank), where ODP Hole 735B is drilled (after Natland and Dick, 2002).

that the kinked  $\text{TiO}_2\text{-Mg}_{\text{Cpx}}^{\#}$  and  $\text{Na}_2\text{O-Mg}_{\text{Cpx}}^{\#}$  systematics in cpx are straightforward consequences of parental MORB melt evolution and liquidus mineral stoichiometric control. This differs from the model of *in situ* boundary layer crystallization (Casey et al., 2007) within a fully convecting steady-state magma chamber that is inconsistent with the observation that melt emplacement takes the form of thin sills at the slow-spreading SWIR (e.g., Dick et al., 2000, 2002; Niu et al., 2002a; Bloomer et al., 1989).

## 2. Geological context of ODP Hole 735B

ODP Hole 735B is drilled into the Atlantis Bank, the shoulder of the Atlantis II transform at the SWIR, southeast of Madagascar. The Atlantis Bank is a tectonically exposed lower oceanic crustal block, permitting drilling into the lower crustal lithologies with the least technical difficulties (Fig. 1). This study uses existing data on samples

recovered from Hole 735B and collated by Dick et al. (2002). Hole 735B was initiated during Leg 118 in 1987 and penetrated 508 m (Robinson et al., 1989), and was further deepened to 1508 m during Leg 176 in 1997 (see Natland and Dick, 2002). An additional hole (1105A) in the vicinity of Hole 735B was initiated during Leg 179 with a penetration of 154 m (see Casey et al., 2007) in order to gather more information on the oceanic lower crust from this otherwise inaccessible and poorly understood realm.

Gabbroic sections of ophiolites tectonically obducted on land have long been thought to represent the lower oceanic crust. However, data collected from Hole 735B show many differences as well as similarities to ophiolite gabbros (Dick et al., 1999, 2000). The Hole 735B sequence consists of hundreds of texturally and mineralogically distinct “layers” with gradational or sutured contacts. These observations are inconsistent with being produced by a large steady-state magma chamber, but are consistent with being solidified from magma lenses of

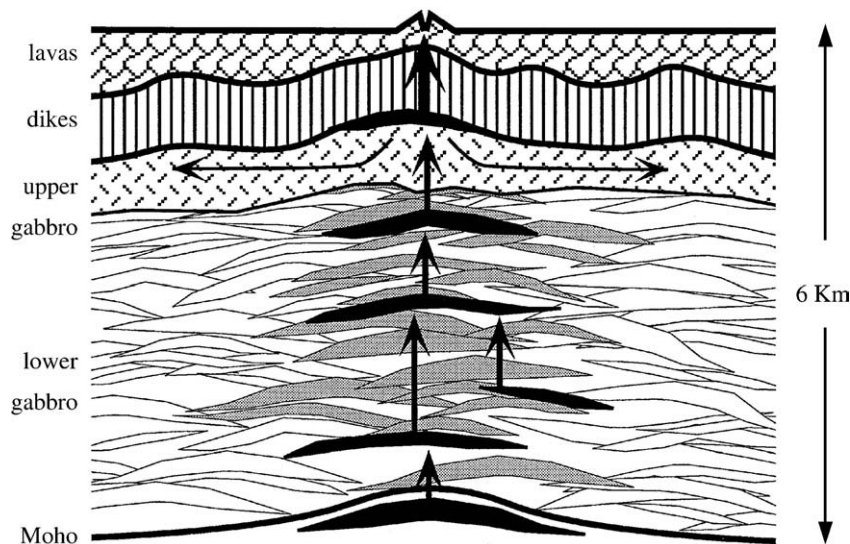


**Fig. 2.** “Sheeted Sills” model for ocean crust formation on the basis of Oman ophiolite, showing melt transport via hydro-fractures and on-axis sill intrusions (Korenaga and Kelemen, 1998; MacLeod and Yaouancq, 2000). The drill core stratigraphy and lithological variations of ODP Hole 735B are consistent with this ocean crust emplacement model (e.g., Dick et al., 2000; Natland and Dick, 2002; Dick et al., 2002; Niu et al., 2002a; after Korenaga and Kelemen, 1998).

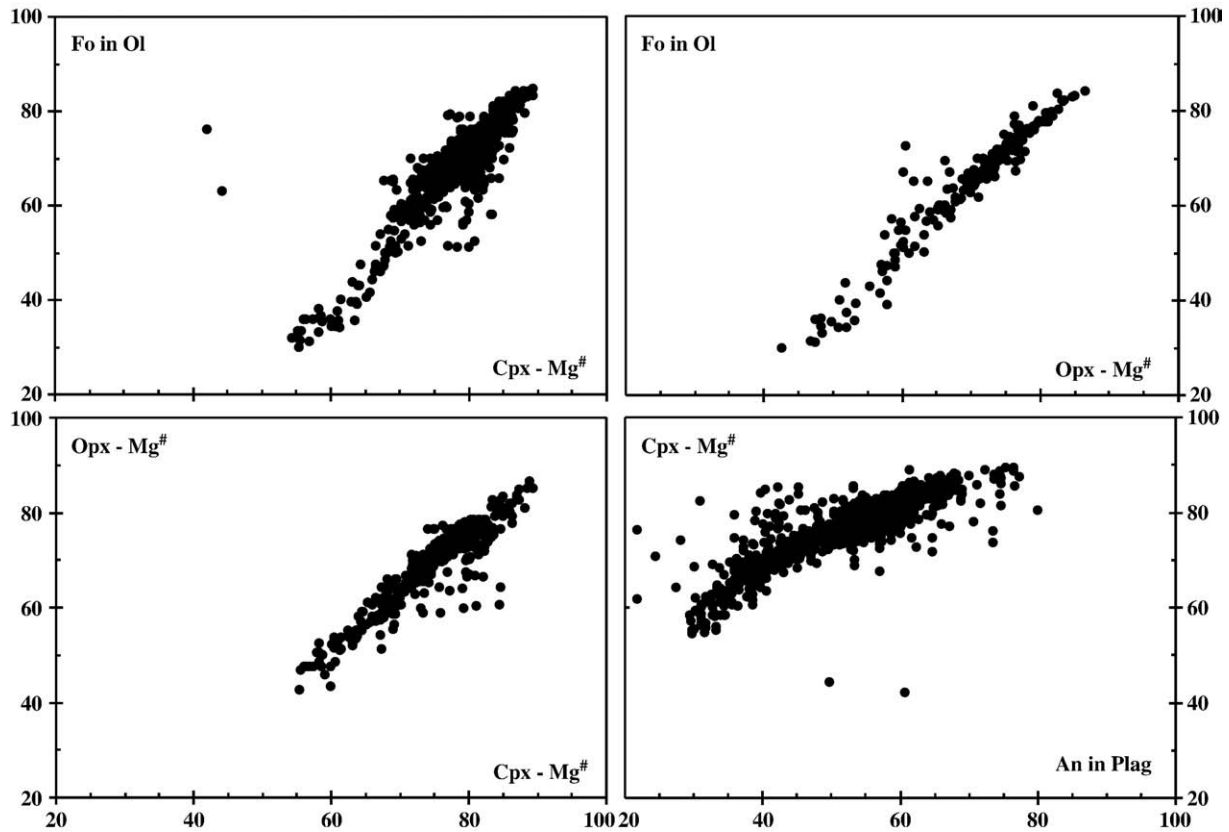


**Fig. 3.** Plots of correlated variations of olivine (ol) forsterite (Fo) content (the same as  $Mg^{\#} = Mg/[Mg+Fe^{2+}]$ ),  $Mg^{\#}$  of orthopyroxene (opx) and clinopyroxene (cpx), and plagioclase (plag) anorthite (An) content to show first order compositional equilibria among coexisting major mineral phases in Hole 735B gabbros and gabbroic rocks. Note that the kind in  $Mg_{Cpx}^{\#}$  vs.  $An_{Plag}^{\#}$  with  $Mg_{Cpx}^{\#} < 0.70$  and  $An_{Plag}^{\#} < 0.40$  reflects cpx–plag equilibria at highly evolved felsic melt. Data are from the compilation of Niu et al. (2002a) and Dick et al. (2002).

multiple melt injections (e.g., Bloomer et al., 1989; Korenaga and Kelemen, 1998; MacLeod and Yaouancq, 2000; Dick et al., 2000, 2002; Niu et al., 2002a). The latter is best described by the “sheeted sills” model (see Fig. 2) proposed to form the ocean crust whereby melt is supplied to a crystal “mush” zone via small (<1 m) melt lenses or sills (Korenaga and Kelemen, 1998; MacLeod and Yaouancq, 2000). Such melt lenses are thermally short-lived (e.g., Annen et al., 2006) and cannot develop magma chambers traditionally perceived to have thermal and compositional boundary layers advocated by Casey et al. (2007) to explain the cpx compositional variations. It is important to note that the “sheeted sills” model was based on observations of the Oman ophiolite interpreted to resemble scenarios of fast-spreading ridges with frequent melt supply (Korenaga and Kelemen, 1998; MacLeod and Yaouancq, 2000). Hence, it is less likely that long-lived steady-state magma chambers can develop at slow-spreading ridges such as the SWIR where melt supply is infrequent, as indicated by the Hole 735B observations (e.g., Dick et al., 2000, 2002). Apparently, the mechanism of multiple-sill emplacement is physically more plausible even for large granitic intrusive complexes (e.g., Annen et al., 2006).

### 3. Data and documentations

Dick et al. (2002) compiled all the compositional data of the constituent mineral phases (olivine, plagioclase, clinopyroxene, oxide minerals and amphibole as well as other minor phases) of the entire Hole 735B gabbroic mass recovered during Leg 118 (0–500 mbsf; Dick et al., 1991) and Leg 176 (500–1508 mbsf; Natland and Dick, 2002). A total of 7371 clinopyroxene (cpx) and plagioclase (plag) analyses were obtained throughout the hole. The total number of analyses for olivine (oliv), orthopyroxene (opx), oxides, amphiboles and minor phases is less due to their absence in many samples. These individual analyses represent a total of 1041 “samples” collected as a function of down-hole depth as

described by Dick et al. (2002). While the mineral data have all been collected using electron microprobe technique in each laboratory with international mineral standards, an inter-laboratory comparison was not straightforward as the data was collected over an 11 year period (see Dick et al., 2002 for more details). However, the mineral compositional variations are not due to inter-laboratory discrepancies if any (Dick et al., 2002). For example, the small data set reported by Casey et al. (2007) from Hole 1105A was collected in a single laboratory, but shows the same mineral compositional systematics. In this study, we only use Hole 735B data, i.e., both the 7371 individual analyses and the 1041 “sample averages” by Dick et al. (2002) to illustrate the concepts. We do not include the small data set by Casey et al. (2007) from the shallow (154 m) Hole 1105A drilled 1 km northeast of Hole 735B, nor oceanic gabbro data from elsewhere (see Coogan, 2007). Despite the shallower depth (and hence smaller sample size), cpx data from Hole 1105A (Casey et al., 2007) shows similar compositional systematics to that of Hole 735B. This suggests that the mineral compositional data of Hole 735B are probably representative of oceanic gabbros and gabbroic rocks in general, although detailed lithostratigraphy may vary from one location to another.

As reported by Niu et al. (2002a) and Dick et al. (2002), while there exist large mineral compositional variations throughout the 1508 m hole, there also exist first order correlated variations among coexisting minerals such as  $Mg^{\#}$  (i.e.,  $Mg/[Mg+Fe^{2+}]$ ) of oliv, cpx, opx and An (i.e.,  $Ca/[Ca+Na]$ ) of plag as summarized in Fig. 3. Because oliv, plag, and to a lesser extent, opx are simple solid solutions, their internal major element compositional variations are readily understood in terms of end-member components and their expected complementarities. However, cpx shows large compositional variations (Fig. 4; also see Dick et al., 2002).

Fig. 4 plots FeO,  $Al_2O_3$ , CaO,  $TiO_2$ ,  $Na_2O$  and  $Cr_2O_3$  (wt.%) in cpx against  $Mg_{Cpx}^{\#}$ . Obviously, FeO,  $Al_2O_3$ , CaO and  $Cr_2O_3$  exhibit straightforward trends with  $Mg_{Cpx}^{\#}$  in terms of the known liquid

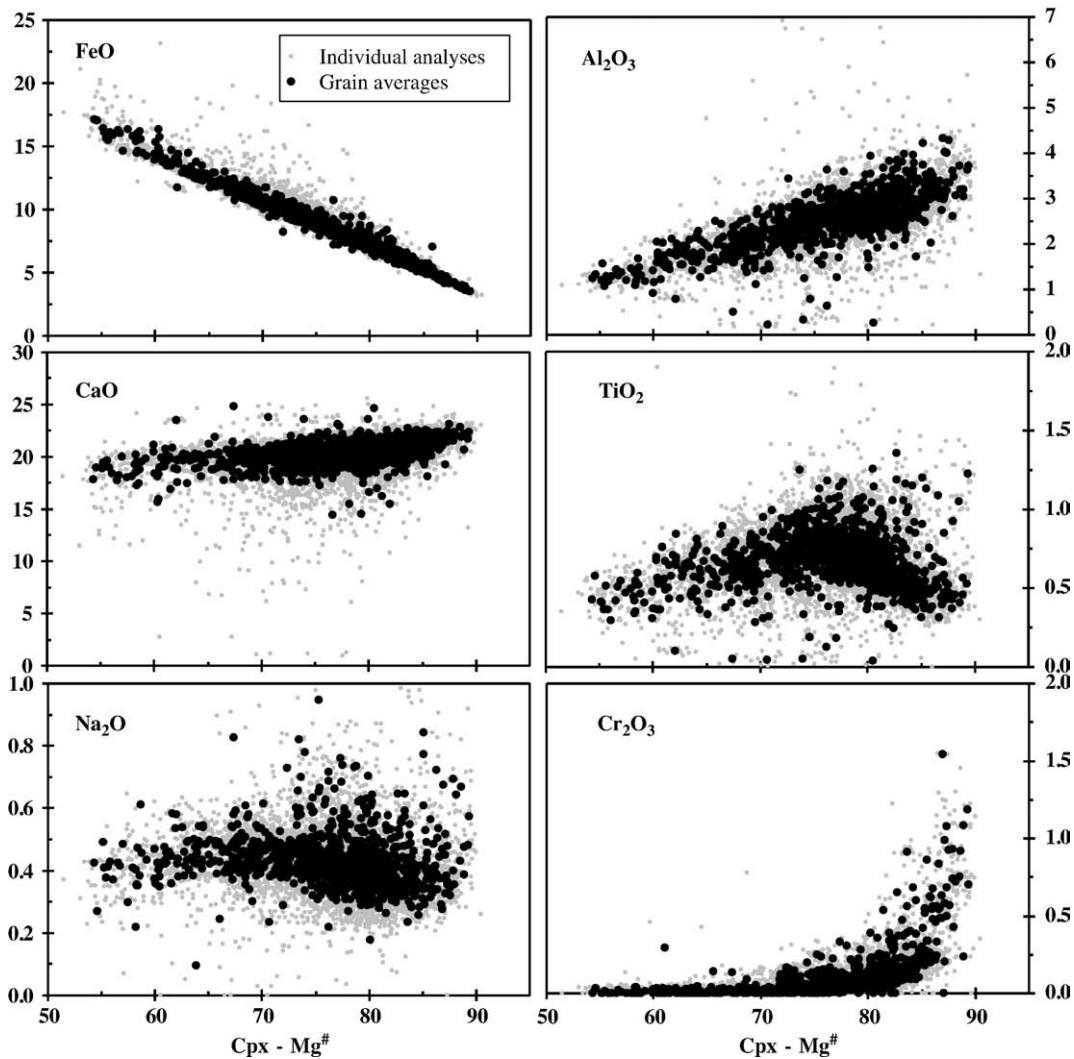


**Fig. 4.**  $Mg_{\text{Cpx}}^{\#}$  variation diagrams of FeO,  $Al_2O_3$ , CaO,  $TiO_2$ ,  $Na_2O$  and  $Cr_2O_3$  to show cpx compositional systematics as a function of liquidus temperature of the parental MORB melt approximated by  $Mg_{\text{Cpx}}^{\#}$  (see Figs. 6 and 7). Small grey symbols are individual analyses and large black symbols are grain averages. The inverse FeO– $Mg^{\#}$  trend, though self-correlated because of  $Mg^{\#} = Mg/[Mg+Fe^{2+}]$ , is purposely plotted to show data coherence, and to show that FeO variation has no effect on  $TiO_2$  and  $Na_2O$  variation, but  $Cr_2O_3$  does. Data from Dick et al. (2002).

lines of descent (LLDs; Fig. 5). However,  $TiO_2$  and  $Na_2O$  show “unexpected” curves or kinks (Dick et al., 2002; Casey et al., 2007) in terms of the known LLDs (Casey et al., 2007). Thy (2003) noted the “oddities” of the data are not caused by Fe related data closure. Dick et al. (2002) pointed out that the declining  $TiO_2$  at lower  $Mg_{\text{Cpx}}^{\#}$  (at  $Mg_{\text{Cpx}}^{\#} \leq 0.75 \pm 0.01$  shown here) is perhaps due to oxide crystallization from the melt, but offered no explanation why  $TiO_2$  increases with decreasing  $Mg_{\text{Cpx}}^{\#}$  at the high  $Mg_{\text{Cpx}}^{\#}$  range nor to the  $Na_2O$  variation, where the trend flattens at  $Mg_{\text{Cpx}}^{\#} \leq 0.73$ . Thy (2003) noted the similar variations in cpx from ODP Hole 1105A on a smaller data set (15–154 mbsf), and suggested that the  $TiO_2$  variation could be due to stoichiometric control (e.g.,  $TiAl_2 \leftrightarrow [Mg, Fe^{2+}]Si_2$ ) without considering the effect of  $Cr_2O_3$  and  $Al_2O_3$  (see below). Casey et al. (2007) used the Hole 1105A samples to argue that the kinked cpx  $Mg_{\text{Cpx}}^{\#}$ – $TiO_2$  and  $Mg_{\text{Cpx}}^{\#}$ – $Na_2O$  trends result from *in situ* crystallization in a steady-state magma chamber whereby a thermal and compositional boundary layer may develop against the roof or side wall of the magma chamber (e.g., McBirney and Noyes, 1979; Langmuir, 1989; Nielsen and Delong, 1992).

We consider that the *in situ* crystallization interpretation (Casey et al., 2007) is theoretically attractive, but is unlikely in reality because the drill hole observations are consistent with the model of “multiple injections and melt lenses (<1 m)” (Fig. 2; e.g., Korenaga and

Kelemen, 1998; Bloomer et al., 1989; MacLeod and Yaouancq, 2000; Dick et al., 2000; Niu et al., 2002a;) and show no evidence for the presence of large enough steady-state magma chambers for developing thermal and compositional boundary layers. Melt emplacement by means of multiple injections of thin melt lenses (vs. large magma chambers) is consistent with reduced extent of mantle melting and infrequent melt supply to the crust at slow-spreading ridges (e.g., Niu and Hékinian, 1997a; Niu, 1997).

The “unexpected”  $Na_2O$  and  $TiO_2$  behaviour in cpx could be ascribed to pressure-dependent partition coefficients of these two elements during basaltic melt evolution (Elthon et al., 1992). While  $Kd$ 's for Ti and Na between cpx and melt are higher at higher pressures (>3–10 kbars; Elthon et al., 1992), it is unclear how this affects the observed cpx  $Na_2O$  and  $TiO_2$  behaviour that is clearly compositional (cpx and thus parental melt) dependent (Figs. 4 and 5). Furthermore, the Hole 735B gabbroic lithologies are likely emplaced at deep crustal levels at pressures <2 kbars. Coogan (2007) suggests that late state crystallization of trapped more evolved liquids can affect mineral compositions in finally solidified gabbroic rocks. This may be true but still cannot explain the observed  $Mg_{\text{Cpx}}^{\#}$ – $TiO_2$  and  $Mg_{\text{Cpx}}^{\#}$ – $Na_2O$  systematics in cpx that is probably a general feature of gabbroic cpx as it is not only seen in Hole 735B and Hole 1105A (Casey et al., 2007), but also in oceanic gabbros from elsewhere (Coogan, Pers. Comm.

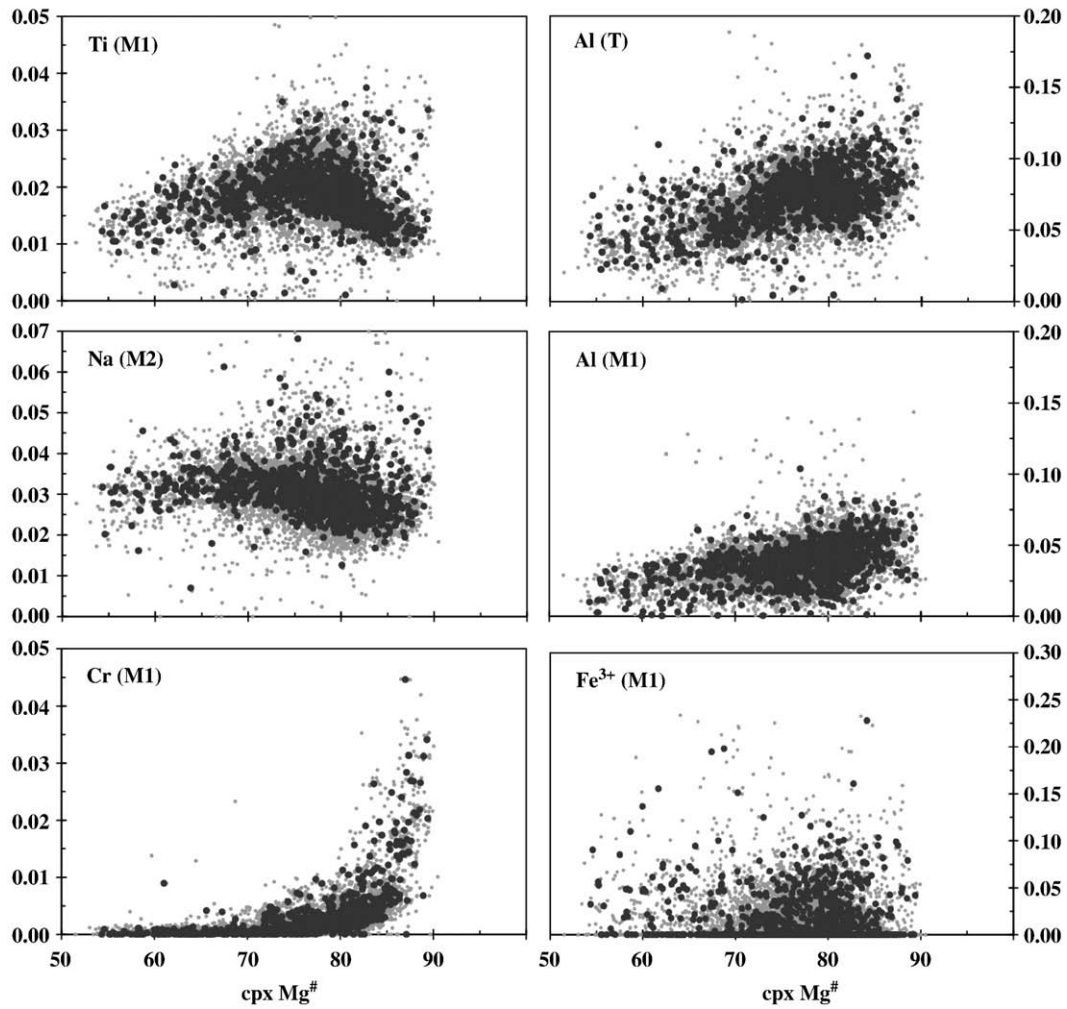


**Fig. 5.** Plots of relevant cations (Ti, Al, Na, Cr and  $\text{Fe}^{3+}$ ) on cpx M1, M2 and T sites as a function of  $\text{Mg}_{\text{Cpx}}^{\#}$  (as in Fig. 4). The cation calculation procedure is given in Section 4.2. Note that  $\text{Fe}^{3+}[\text{M1}]$  does not correlate with any other parameters and thus cannot be the cause of Ti and Na systematics with  $\text{Mg}_{\text{Cpx}}^{\#}$ . Because the topologies of Na[M2], Ti[M1] and Cr[M1] resemble those of  $\text{Na}_2\text{O}$ ,  $\text{TiO}_2$  and  $\text{Cr}_2\text{O}_3$  in Fig. 4, we discuss cpx compositional variation and liquid lines of descent (LLDs) using wt.% oxides to be consistent with the same use for melt compositions (Figs. 6 and 7).

2008). It is also worth to point out that the compositional scatter in Fig. 4 may be caused by varying amounts of trapped liquids, but our aim is to understand the first-order trends.

We also plot relevant cations of interest Al[M1], Al[T], Ti[M1], Na[M2], Cr[M1] and  $\text{Fe}^{3+}[\text{M1}]$  as a function of  $\text{Mg}_{\text{Cpx}}^{\#}$  in Fig. 5 (see Section 4.2 below for calculation procedure). As their topologies are identical to  $\text{TiO}_2$ – $\text{Mg}_{\text{Cpx}}^{\#}$ ,  $\text{Na}_2\text{O}$ – $\text{Mg}_{\text{Cpx}}^{\#}$  and  $\text{Cr}_2\text{O}_3$ – $\text{Mg}_{\text{Cpx}}^{\#}$  in Fig. 4, we will use the latter (oxides wt.%) in discussing mineral compositional systematics in terms of LLDs (see below).

#### 4. Our interpretations

##### 4.1. Liquid lines of descent (LLDs)

As these gabbros (and gabbroic rocks) are largely co-precipitates of cpx and plag (plus other minerals at appropriate liquidus temperatures) from cooling MORB melts, it is logical to first examine LLDs of a MORB melt, which helps understand the sequence of liquidus phase (e.g., oliv, plag, cpx) appearance, and the compositional changes of these phases as the melt cools and evolves.

Fig. 6 shows LLDs of MORB melts for  $\text{SiO}_2$ ,  $\text{TiO}_2$ ,  $\text{Al}_2\text{O}_3$ ,  $\text{FeO}$ ,  $\text{CaO}$ ,  $\text{Na}_2\text{O}$  and  $\text{Cr}_2\text{O}_3$  as a function of MORB  $\text{Mg}^{\#}$  ( $=\text{Mg}/[\text{Mg} + \text{Fe}]$ ) or liquidus temperature ( $^{\circ}\text{C}$ ) (Also see Fig. F2 of Niu et al., 2002a and Fig. 6 caption). Fig. 6 says that as the melt cools (decreasing  $\text{Mg}^{\#}$  from right to the left),

the compositional variation trends of the remaining liquid reflect the effects of minerals that have crystallized and separated. This is readily seen from the bottom two panels. For example, from this set of the data we see that olivine is already on the liquidus and crystallizing at  $\text{Mg}_{\text{Melt}}^{\#} \approx 0.72$ ,  $\sim 1240 \pm 10$   $^{\circ}\text{C}$  (this 10  $^{\circ}\text{C}$  uncertainty resulted from experimental data regression, see Niu et al., 2002a; Niu, 2005). Crystallization of olivine with chromite would produce dunite (this explains the genetic association of chromite mineralization with dunite). At  $\text{Mg}_{\text{Melt}}^{\#} \approx 0.69$ ,  $\sim 1222 \pm 10$   $^{\circ}\text{C}$ , plag joins olivine to form troctolite (e.g. plag + oliv rock). At  $\text{Mg}_{\text{Melt}}^{\#} \approx 0.58$ ,  $\sim 1180 \pm 10$   $^{\circ}\text{C}$ , cpx joins plag (and oliv) to form gabbros (plag + cpx + oliv rock). At an even lower temperature,  $\sim 1115 \pm 10$   $^{\circ}\text{C}$  with  $\text{Mg}_{\text{Melt}}^{\#} \approx 0.37$ , Ti–Fe oxides begin to crystallize (with or without cpx and fayalitic oliv), forming Fe–Ti oxide gabbros, gabbro-norite etc. (this explains the genetic associations of V–Ti–Fe mineralization with highly evolved gabbro or gabbro-norite). Note that apatite, and perhaps zircons, may crystallize at this late stage of tholeiitic magma evolution (Niu et al., 2002a; Niu, 2005). It is important to note that it is Fe–Ti oxide crystallization that drives the enrichment of  $\text{SiO}_2$  in the residual melt (Fig. 5), i.e., the basaltic–andesite stage of tholeiitic melt evolution (see Fig. F4 of Niu et al., 2002a; Danyushevsky, 1998). This  $\text{SiO}_2$  enrichment leads to the production of volumetrically small ( $\sim 0.5$  vol.%) but widespread felsic vein lithologies (tonalitic, trondhjemitic, dioritic and granitic veins/veinlets) in Hole 735B (see Fig. F4 of Niu et al.,

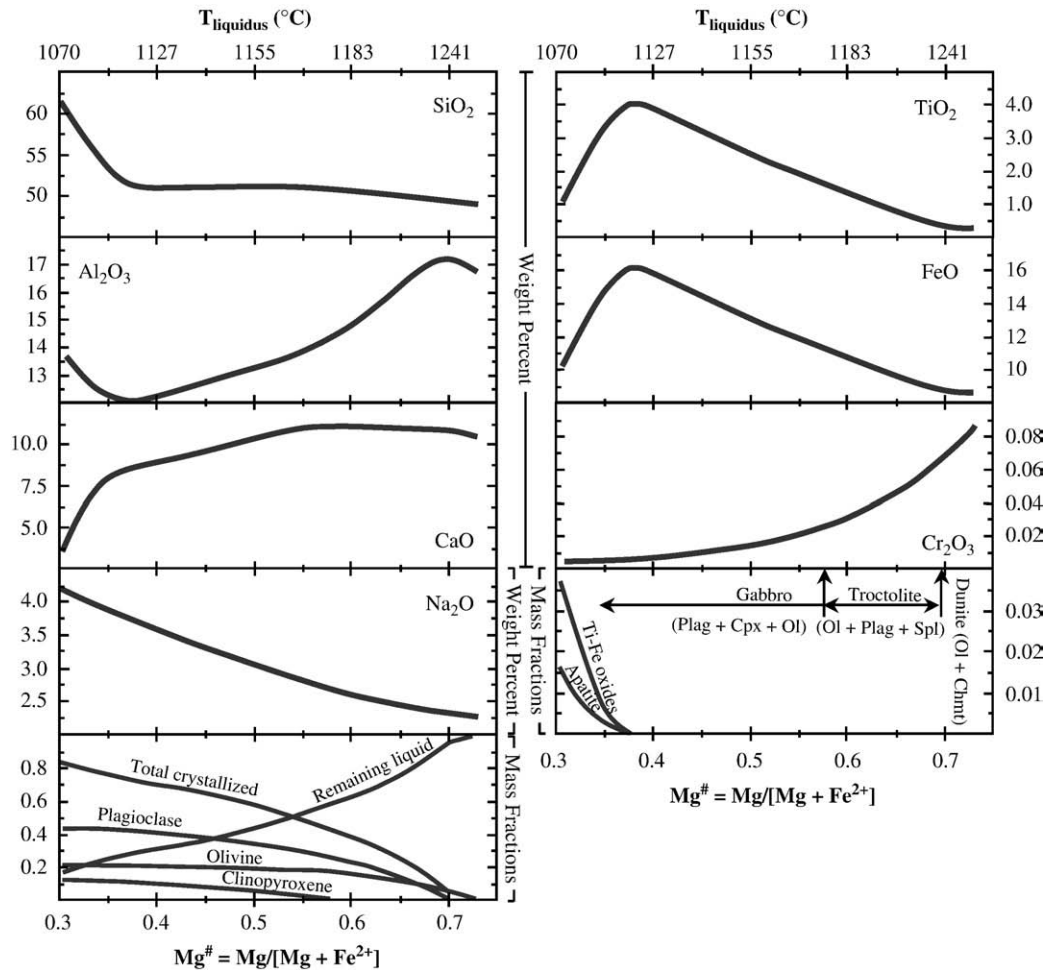


**Fig. 6.** Liquid lines of descent (LLDs) derived from >400 N-type anhydrous MORB melts from the East Pacific Rise and nearby seamounts (Batiza et al., 1989, 1990; Batiza and Niu, 1992; Niu and Batiza, 1997; Niu et al., 1996, 1999; 2002b; Regelous et al., 1999; Batiza et al., 1989, 1990; Batiza and Niu, 1992; Niu and Batiza, 1997; Niu et al., 1999; 2002b; Regelous et al., 1999; Niu, 2005; Niu and O'Hara, 2008) and experimental data (see Fig. F2 of Niu et al., 2002a for reference details) for  $\text{SiO}_2$ ,  $\text{Al}_2\text{O}_3$ ,  $\text{CaO}$ ,  $\text{FeO}$ ,  $\text{TiO}_2$ ,  $\text{Na}_2\text{O}$ ,  $\text{Cr}_2\text{O}_3$  and liquidus phase proportions with decreasing  $\text{Mg}_{\text{Melt}}^{\#}$  (modified from Niu, 2005). Note that cpx begins to crystallize late (vs. ol and plag) at  $\text{Mg}_{\text{Melt}}^{\#} \sim 0.57$ , i.e., gabbros and the more evolved lithologies represent relatively late-stage basaltic magma evolution. The liquidus temperature ( $\pm 10^\circ\text{C}$  uncertainties) and appearance and proportions of liquidus phases are determined using low pressure (1 bar) experiments to illustrate the concept (see Niu et al., 2002a; Niu, 2005). At higher pressures, cpx may begin to crystallize earlier. These compare well with the widely used empirical LLD models by Weaver and Langmuir (1990) and Danyushevsky (1998) (see Figs. F3 and F4 of Niu et al., 2002a for details).

2002a). Note that Fig. 6 is meant to illustrate the concept and by no means represents exact compositions of MORB melts parental to the Hole 735B gabbroic lithologies.

Note also that when calculating MORB melt  $\text{Mg}^{\#} = \text{Mg}/[\text{Mg} + \text{Fe}^{2+}]$ , we assume 10% total Fe as  $\text{Fe}^{3+}$  appropriate for MORB (Christie et al., 1986) without making further assumptions on oxygen fugacity ( $f\text{O}_2$ ) that is not well constrained during MORB melt evolution. We calculated  $\text{Mg}_{\text{Cpx}}^{\#}$  similarly ( $\text{Mg}^{\#} = \text{Mg}/[\text{Mg} + \text{Fe}^{2+}]$ ) by obtaining  $\text{Fe}^{3+}$  from total Fe ( $=\text{Fe}^{2+} + \text{Fe}^{3+}$ ) using charge balance and stoichiometry (see below). Note that the calculated  $\text{Fe}^{3+}$  occupying the cpx M1 site shows no systematic variation with  $\text{Mg}_{\text{Cpx}}^{\#}$ , suggesting that  $\text{Fe}^{3+}$  in cpx is not the cause of Ti and Na behaviour in cpx (Fig. 5). That is, the observed  $\text{TiO}_2$ - $\text{Mg}_{\text{Cpx}}^{\#}$  and  $\text{Na}_2\text{O}$ - $\text{Mg}_{\text{Cpx}}^{\#}$  kinks in cpx are clearly unrelated to  $\text{Fe}^{3+}$  (Fig. 5), but genetically associated with  $\text{Cr}_2\text{O}_3$  (Figs. 4 and 5).

An important point here is that gabbros are the product of basaltic magma evolution at relatively lower temperatures ( $< \sim 1180 \pm 10^\circ\text{C}$ ) when cpx joins plag and olivine on the liquidus (Fig. 6). The olivine-basaltic melt phase equilibrium at low pressure (crystal vs. mantle) is well constrained by  $K_D^{\text{Ol/Melt}} = [X_{\text{Ol}}^{\text{FeO}}/X_{\text{Melt}}^{\text{FeO}}]/[X_{\text{Ol}}^{\text{MgO}}/X_{\text{Melt}}^{\text{MgO}}] = 0.3 \pm 0.03$  (Roeder and Emslie, 1970). It is also known that  $\text{Mg}_{\text{Cpx}}^{\#} > \text{Mg}_{\text{Ol}}^{\#}$ , and we obtained  $K_D^{\text{DCpx/Melt}} \sim 0.22$  by considering experimental data (e.g., Grove et al., 1992) and  $\text{Mg}_{\text{Cpx}}^{\#}/\text{Mg}_{\text{Ol}}^{\#}$  ratios of the data set (see Fig. 3 and also Niu et al., 2002a).

Fig. 7a shows the relationship between  $\text{Mg}_{\text{Cpx}}^{\#}$  and  $\text{Mg}_{\text{Melt}}^{\#}$  (thick grey line) using  $K_D^{\text{Cpx/melt}} \sim 0.22$ . Fig. 7b and c compare  $\text{Mg}_{\text{Cpx}}^{\#}$  with  $\text{Mg}_{\text{Melt}}^{\#}$  (horizontal axis) using  $\text{Al}_2\text{O}_3$  (vertical axis) as an example in cpx (Fig. 7b) and in equilibrium melt (Fig. 7c). Fig. 7b and c show explicitly that most cpx crystals from Hole 735B that we study crystallized from quite evolved melt with  $\text{Mg}_{\text{Melt}}^{\#} = 0.58$  to 0.40 (gabbroic fractionation), significant amount of cpx crystallized from the even more evolved melt with  $\text{Mg}_{\text{Melt}}^{\#} = 0.40$  to 0.30 that produced oxide gabbro or gabbro-norite, and still some cpx crystallized from highly evolved felsic melt with  $\text{Mg}_{\text{Melt}}^{\#} < 0.3$ . The most evolved cpx with  $\text{Mg}_{\text{Cpx}}^{\#} \approx 0.55$  would be in equilibrium with felsic melt having  $\text{Mg}_{\text{Melt}}^{\#} \sim 0.21$ , which would also have Na-rich plag and other granitic phase assemblages on the liquidus as observed (Niu et al., 2002a). This is a critically important observation for understanding minor element systematics in cpx that we study, but has apparently been neglected previously (Thy, 2003; Casey et al., 2007) (see below).

#### 4.2. Clinopyroxene stoichiometry and elemental compatibility

Fig. 8a shows the generally accepted elemental occupancy in cpx structure (e.g., Cameron and Papike, 1980). It is particularly important to note that  $\text{Na}^+$  occupies M2 site only, and  $\text{Ti}^{4+}$   $\text{Cr}^{3+}$

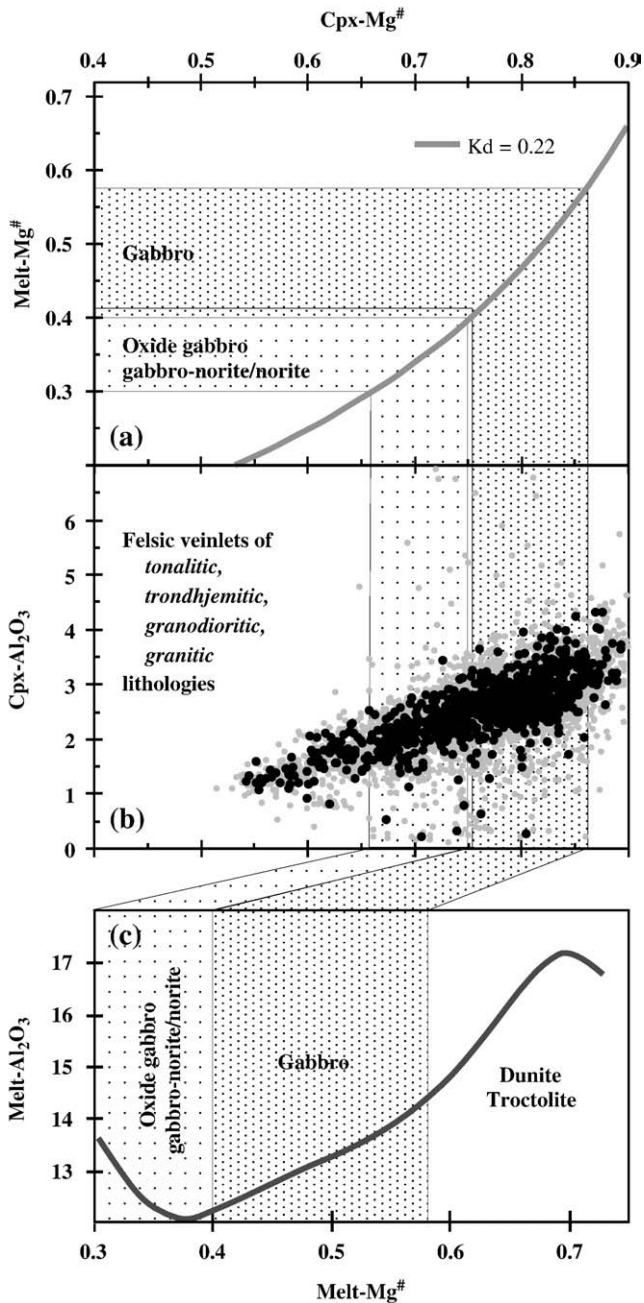


**Fig. 7.** (a) shows that  $Mg_{Cpx}^{\#}$  and  $Mg_{Melt}^{\#}$  are related by  $K_D^{cpx/melt} = [FeO/MgO]^{cpx}/[FeO/MgO]^{melt} = -0.22$  obtained by considering experimental data (e.g., Grove et al., 1992) and  $Mg_{Cpx}^{\#}/Mg_{O1}^{\#}$  ratios of the data set (see Fig. 3), and thus both are proportional to the liquidus temperature (see Fig. 6). (b) plots  $cpx-Al_2O_3$  vs.  $Mg_{Cpx}^{\#}$  to compare with  $melt-Al_2O_3$  vs.  $Mg_{Melt}^{\#}$  in (c) reproduced from Fig. 6. The liquidus fields indicated are as in the lower panels of Fig. 6.

and  $Fe^{3+}$  occupy M1 site only, whereas  $Al^{3+}$  occupies both M1 and T sites. Using a structural formula of the form  $[M2]_1[M1]_1T_2O_6$ , we distribute cations as follows (e.g., Morimoto, 1988):

- [1] Si enters T site with the remaining space (i.e., 2-Si) filled with Al;
- [2] The remainder Al enters M1 site;
- [3] All Ti and Cr enter M1 site, and all Na, Ca and Mn enter M2 site;
- [4] Total Fe is recast to  $Fe^{2+}$  and  $Fe^{3+}$  by charge balance with  $Fe^{3+}$  entering M1 site;
- [5]  $Fe^{2+}$  and Mg are apportioned between remaining spaces on M2 and M1 sites. That is,  $(1-[M1]) \times Fe^{2+}/(Fe^{2+}+Mg)$  for  $Fe^{2+}$  and  $(1-[M1]) \times Mg/(Fe^{2+}+Mg)$  for Mg on M1 site.  $(1-[M2]) \times Fe^{2+}/$

$(Fe^{2+}+Mg)$  for  $Fe^{2+}$  and  $(1-[M2]) \times Mg/(Fe^{2+}+Mg)$  for Mg on M2 site, where [M1] and [M2] refer to the sum of non- $Fe^{2+}$  and non-Mg cations on M1 and M2 sites respectively.

Fig. 8b shows several possible charge-balanced stoichiometric combinations of non- $M^{2+}$  cations of interest, i.e.,  $Na^+$ ,  $Ti^{4+}$ ,  $Al^{3+}$ ,  $Cr^{3+}$  and  $Si^{4+}$  in cpx.  $Fe^{3+}$  is not considered because although the relative abundance of  $Fe^{3+}$  [M1] is high, it does not show systematic variation with  $Mg_{Cpx}^{\#}$  (Fig. 5) and thus does not control the systematics of other cations, in particular,  $Ti^{4+}$ ,  $Na^+$  and  $Cr^{3+}$ , which we endeavour to understand.

Cr is highly compatible ( $K_D^{cpx/melt} \sim 3.5$ ; Hart and Dunn, 1993) whereas Ti ( $K_D^{cpx/melt} \sim 0.30$ ) and Na ( $K_D^{cpx/melt} \sim 0.15$ ) (Langmuir et al., 1992) are incompatible in cpx that is crystallizing from the cooling basaltic melt. It follows that Cr has the strong tendency to enter the crystallizing cpx while Ti and Na prefer to stay in the residual melt (vs. the crystallizing cpx). These apparent distribution coefficients are consistent with their LLDs (Fig. 6). In Fig. 6, the rapid decrease of Cr with decreasing  $Mg_{Melt}^{\#}$  at high  $Mg^{\#}$  values results from Cr-spinel crystallization (Niu, 2005), and its continued decrease at low  $Mg_{Melt}^{\#}$  values is consistent with cpx crystallization. In fact, the increase of  $TiO_2$  and  $Na_2O$  with decreasing  $Mg_{Melt}^{\#}$  in the residual melt is consistent with Ti and Na being incompatible in all the major liquidus phases (Fig. 6) including olivine, cpx and Ca-rich plagioclase.

The rapid  $Cr_2O_3$  decrease in cpx with decreasing  $Mg_{Cpx}^{\#}$  (Fig. 4) results from Cr depletion in the melt due to continued cpx crystallization, resulting, in turn, from its high compatibility in cpx (Fig. 6). As both Cr and Ti occupy M1 site in cpx, the amount of Ti that can reside on M1 site must be complementary to Cr (see Fig. 4). Hence, Ti increase is associated with Cr decrease in cpx as the melt cools and cpx continues to crystallize from the progressively more evolved melts (producing lowered  $Mg_{Cpx}^{\#}$ ). This explains why  $TiO_2$  reaches the maximum when Cr diminishes at  $Mg_{Cpx}^{\#} \approx 0.76 \pm 0.01$  in cpx (Fig. 4), which is equivalent to  $Mg_{Melt}^{\#} \approx 0.41 \pm 0.01$  in the melt (Fig. 7a). At  $Mg_{Melt}^{\#} \sim 0.39 \pm 0.01$  (Fig. 6), Fe–Ti oxides begin to crystallize, which depletes Ti (as well as Fe; Fig. 6) in the residual melt and makes Ti progressively less available for cpx. Hence,  $TiO_2$  decreases in cpx with decreasing  $Mg_{Cpx}^{\#}$  at low  $Mg^{\#}$  values (Figs. 4 and 5). The lack of apparent FeO decrease in Fig. 4 is due to the artifact that  $Mg_{Cpx}^{\#}$  is calculated from both FeO and MgO in cpx (i.e.,  $Mg_{Cpx}^{\#} = Mg/[Mg+Fe^{2+}]$ ) while both FeO and MgO decrease. As discussed above (Fig. 5),  $Fe^{3+}$  does not correlate with any other cations and is thus not the cause of the observed Ti, Cr and Na systematics (Figs. 4 and 5). Fig. 4 demonstrates the complementary relationship of  $TiO_2$  (and to a lesser extent of  $Na_2O$ ) with  $Cr_2O_3$ , but not with FeO, and Fig. 5 shows the complementary relationship of Ti (M1) with Cr (M1), but not with  $Fe^{3+}$  (M1).

Fig. 6 shows that  $Na_2O$  in the crystallizing cpx should increase with decreasing  $Mg_{Cpx}^{\#}$  because  $Na_2O$  in the melt apparently increases with decreasing  $Mg_{Melt}^{\#}$ . Caution is, however, necessary here.  $Na_2O$  in cpx does increase with decreasing  $Mg_{Cpx}^{\#}$  at high  $Mg_{Cpx}^{\#}$  values with a peak at  $Mg_{Cpx}^{\#} \approx 0.74$  (Fig. 4), but flattens out at  $Mg_{Cpx}^{\#} \leq 0.73$  (equivalent to  $Mg_{Melt}^{\#} \leq 0.37$ ), which is slightly delayed following the onset of Fe–Ti oxide crystallization at  $Mg_{Melt}^{\#} \approx 0.39 \pm 0.01$  (Fig. 6). This observation points to a genetic link between  $Na_2O$ – $Mg_{Cpx}^{\#}$  flattening and oxide crystallization as is the case for  $TiO_2$  declining (Fig. 4). Melt at  $Mg_{Melt}^{\#} \approx 0.39$  is quite evolved with the liquidus temperature of  $\sim 1100 \pm 10$  °C (Fig. 6), where CaO and  $Al_2O_3$  in the residual melt are sufficiently low,  $Na_2O$ , as an overall incompatible element, is sufficiently high (Fig. 6). The high  $Na_2O$  in the residual melt will make more  $Na_2O$  available for the crystallizing cpx. That is,  $Na_2O$  in cpx should continue to increase with decreasing  $Mg_{Cpx}^{\#}$  (at  $Mg_{Cpx}^{\#} < 0.73$ ), but this is not observed. On the other hand, crystallization of Fe–Ti oxides (at  $Mg_{Cpx}^{\#} < 0.75$  or  $Mg_{Melt}^{\#} < 0.39$ ) leads to  $SiO_2$  jump in the residual melt (Fig. 6) (Niu et al., 2002a; Danyushevsky, 1998). This highly evolved “felsic” melt with high  $Na_2O$  and  $SiO_2$  and low CaO and  $Al_2O_3$  facilitates crystallization of Na-rich (albitic,  $NaAlSi_3O_8$ ) plag. This

is indeed the case in the more evolved felsic vein lithologies from Hole 735B (Niu et al., 2002a). Therefore, Na-rich plag crystallization consumes more Na than before, which will inevitably balance the Na increase in the residual melt, hence leading to the flattened Na<sub>2</sub>O in the co-precipitating cpx, rather than increasing Na<sub>2</sub>O in Na<sub>2</sub>O vs. Mg<sub>Cpx</sub><sup>#</sup> plot at Mg<sub>Cpx</sub><sup>#</sup> ≤ 0.73 (Fig. 4). This conclusion is in fact obvious from Fig. 7b. Melt with Mg<sub>Melt</sub><sup>#</sup> < 0.40, which crystallizes cpx with Mg<sub>Cpx</sub><sup>#</sup> < 0.75, produces oxide gabbro, gabbro-norite, and felsic vein lithologies with Na-rich plagioclase as observed (Niu et al., 2002a). Note that the kink in Mg<sub>Cpx</sub><sup>#</sup> vs. An<sub>Plag</sub><sup>#</sup> diagram at Mg<sub>Cpx</sub><sup>#</sup> < 0.70 and An<sub>Plag</sub><sup>#</sup> < 0.40 in Fig. 3 (also see Fig. F1 of Niu et al., 2002a) reflects the cpx–plag equilibria at highly evolved felsic melt with SiO<sub>2</sub> ≥ 60 wt.% (Niu et al., 2002a). Both Thy (2003) and Casey et al. (2007) neglected to realize that the low Al<sub>2</sub>O<sub>3</sub> and TiO<sub>2</sub> cpx crystals with Mg<sub>Cpx</sub><sup>#</sup> < 0.75 are in fact not liquidus crystals of basaltic melt, but are in equilibrium with felsic melts (after the onset of Fe–Ti oxide crystallization and subsequent SiO<sub>2</sub> enrichment; Fig. 6).

It is worth noting also that Na on M2 site is expected to combine with Al (also Cr and Fe<sup>3+</sup>) on M1 site to form a “jadeitic” component (i.e., NaAlSi<sub>2</sub>O<sub>6</sub> or NaCrSi<sub>2</sub>O<sub>6</sub> or acmitic NaFe<sup>3+</sup>Si<sub>2</sub>O<sub>6</sub>) in cpx. However, the lack of positive correlation between Na on M2 site and Al (also Cr and Fe<sup>3+</sup>) on M1 site (Fig. 9a; also obvious in Fig. 5) suggests that Na does not exist as a jadeitic component, but instead largely charge-balances Ti<sup>4+</sup> and Cr<sup>3+</sup> on

### Proxene Structure Formula: [M2]<sub>1</sub> [M1]<sub>1</sub> [T]<sub>2</sub> O<sub>6</sub>

Crystallographic Site	M2	M1	T
Coordination Number	6 ~ 8	6	4
Cation distribution	Na Ca Li Mn Fe <sup>2+</sup> Mg	Mn Fe <sup>2+</sup> Mg Ti <sup>4+</sup> Cr <sup>3+</sup> Fe <sup>3+</sup> Al	Al Si

(a)

### Proxene Structure and Charge Balance

[M2] <sub>1</sub> + [M1] <sub>1</sub> + T <sub>2</sub> = 12 <sup>+</sup> ; O <sub>6</sub> = 12 <sup>-</sup>		
[M2] <sub>1</sub>	[M1] <sub>1</sub>	[T] <sub>2</sub>
Jadeite: Na <sup>+</sup>	Al <sup>3+</sup>	Si <sub>2</sub> <sup>4+</sup>
Na <sup>+</sup>	Cr <sup>3+</sup>	Si <sub>2</sub> <sup>4+</sup>
Na <sup>+</sup>	Ti <sup>4+</sup>	Al <sup>3+</sup> Si <sub>2</sub> <sup>4+</sup>
(b) Na <sup>+</sup>	Ti <sub>0.5</sub> <sup>4+</sup> Cr <sub>0.5</sub> <sup>3+</sup>	Al <sub>0.5</sub> <sup>3+</sup> Si <sub>1.5</sub> <sup>4+</sup>

Fig. 8. (a) shows generally accepted site preferences of major element cations in cpx (Cameron and Papike, 1980). (b) shows that while several simple and charge-balanced stoichiometric combinations can explain the site occupancies of Na, Cr, Ti, Al and Si, the data do not suggest jadeite (Na[Al,Cr]Si<sub>2</sub>O<sub>6</sub>) as an important component (see Fig. 9a), but favour the charge-balanced combination of Na[Ti<sub>0.5</sub>Cr<sub>0.5</sub>][Al<sub>0.5</sub>Si<sub>1.5</sub>]<sub>2</sub>O<sub>6</sub>, which is the simplest expression to illustrate the concept and the actual combinations are likely more complex when other major cations are considered.

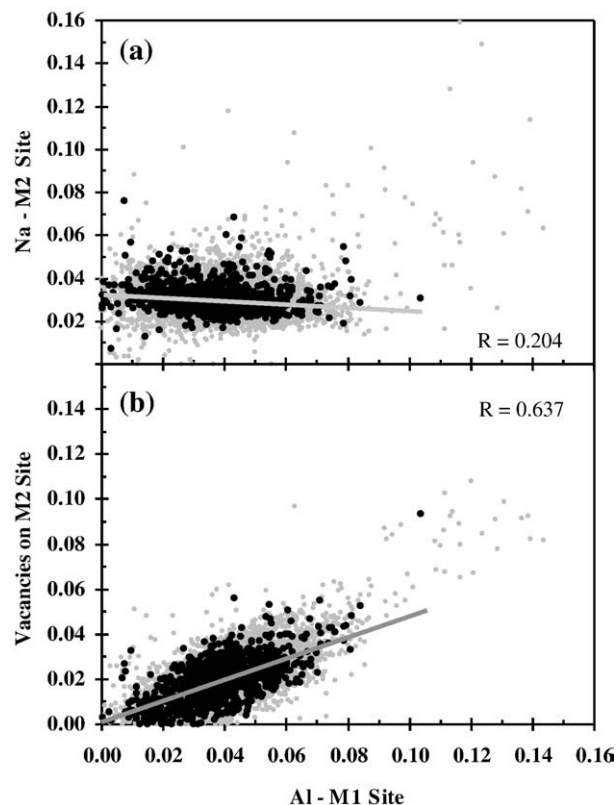


Fig. 9. (a) shows lack of positive correlation between Na on [M2]<sub>1</sub> and Al on [M1]<sub>1</sub>, suggesting Na does not exist as jadeitic component in the cpx, but largely charge-balances Ti<sup>4+</sup> and Cr<sup>3+</sup> (see Fig. 8b). (b) shows a significant positive correlation between “vacancies” on [M2]<sub>1</sub> (after Ca, Mn, Fe<sup>2+</sup> and Mg subtraction from unity) and Al on [M1]<sub>1</sub>. With the essentially zero intercept, the slope of 0.4696 (~Vacancy[M2]<sub>1</sub>/Al[M1]<sub>1</sub>) suggests that to a first order for the entire data set, about half (~47%) of Al[M1]<sub>1</sub> requires charge-balanced by univalent cations such as Na<sup>+</sup> (minute K<sup>+</sup>, Rb<sup>+</sup> etc.) in the form of “jadeitic” component, yet such required amount of univalent cation is missing.

M1 site (Fig. 8b). In fact, on average Al on T site is twice (0.072 ± 0.020; mean ± 1σ) as much as on M1 site (0.039 ± 0.014) (Fig. 5), suggesting that much of the Al in these cpx crystals occurs as complex tschermak components, i.e., [Na,Ca,Mn,Fe,Mg][Ti,Al,Cr,Fe<sup>3+</sup>][Al,Si]<sub>2</sub>O<sub>6</sub>. Also note the significant correlation of “vacancies” on M2 site, which is calculated “Na” by subtracting Ca, Fe<sup>2+</sup>, Mg and Mn on M2 site from unity, with Al on M1 site (Fig. 9b). With the intercept essentially being at zero, the slope of 0.4714 (≈ “Vacancy” [M2]<sub>1</sub>/Al[M1]<sub>1</sub>) suggests that to a first order for the entire data set, about half (~47%) of Al on M1 site is required to be charge-balanced by univalent cations such as Na<sup>+</sup> (plus insignificant K<sup>+</sup>, Rb<sup>+</sup> etc.) on M2 site in the form of “jadeitic” component, yet such required amount of univalent cation is missing. This is not an artefact because calculation of Al on M1 site is independent of cation attribution to M2 site. The origin of the missing univalent cation (i.e., ~0.25 ± 0.07 wt.% on average in terms of Na<sub>2</sub>O for the entire data set) is unclear, but could possibly be due to Na volatilization during probe analysis or subsolidus diffusion loss; further investigation is needed.

However, this suspected Na loss cannot explain the flattening of Na<sub>2</sub>O at Mg<sub>Cpx</sub><sup>#</sup> < 0.73 (Fig. 4) because the “missing Na<sub>2</sub>O” does not correlate with Mg<sub>Cpx</sub><sup>#</sup> or any other parameters. At Mg<sub>Cpx</sub><sup>#</sup> > 0.73, the behaviour of Na is a consequence of two factors: (1) a straightforward cpx/melt partitioning (Na in cpx increases when Na in the melt increases), and (2) coupled charge balance as a passive response to the effect of Cr – Ti coupling, that is, Na<sup>+</sup>Ti<sub>0.5</sub><sup>4+</sup>Cr<sub>0.5</sub><sup>3+</sup>Al<sub>0.5</sub><sup>3+</sup>Si<sub>1.5</sub><sup>4+</sup> (Fig. 8b), which is the simplest form for conceptual clarity, but relative abundances of all these elements actually vary as long as the overall charges are balanced.

## 5. Discussion

We have shown above that the apparently “perplexing”  $\text{TiO}_2$  and  $\text{Na}_2\text{O}$  behaviour in cpx of oceanic lower crust gabbroic lithologies from ODP Hole 735B is a straightforward consequence of tholeiitic melt evolution, dominated by cooling-induced crystallization without the need to invoke complex processes that may not take place in reality. For example, thermal or compositional boundary layer *in situ* crystallization is an elegant concept (e.g., [McBirney and Noyes, 1979](#); [Casey and Karson, 1981](#); [Langmuir, 1989](#); [Nielsen and DeLong, 1992](#); [Casey et al., 2007](#)), but its operation requires perceived magma chambers that are steady-state or large enough in dimension with low enough viscosity to allow vigorous convection. Such a condition is conceivably met in large volumes of melt delivered in a stable tectonic setting such as the formation of layered igneous intrusions. The constant/frequent tectonic activity at ocean ridges is unlikely to allow the development such magma chambers even at fast-spreading ridges like the East Pacific Rise ([Sinton and Detrick, 1992](#)). While magma bodies have been detected in magmatically robust locations along slow-spreading ridges such as the Lucky Strike hydrothermal site at the Mid-Atlantic Ridge ([Singh et al., 2006](#); [Sinha et al., 1997](#)), it is physically unlikely that large steady-state magma chambers can be developed at slow-spreading ridges ([Sinton and Detrick, 1992](#)) due to the reduced extent of mantle melting and infrequent melt supply ([Niu and Hékinian, 1997a,b](#)). Indeed, the litho-stratigraphy of Hole 735B at the slow-spreading SWIR is most consistent with models of “multiple injections and thin melt lenses” (Fig. 2; [Kelemen et al., 1997](#); [Coogan et al., 2000](#); [Natland and Dick, 2002](#); [Dick et al., 2000, 2002](#); [Niu et al., 2002a](#)). Such thin (<1 m) melt lenses readily freeze (e.g., [Annen et al., 2006](#)), let alone be able to develop steady-state magma chambers.

Therefore, the *in situ* boundary layer crystallization model scenario invoked by [Casey et al. \(2007\)](#), though conceptually attractive, is practically ineffective in explaining the observations. [Thy \(2003\)](#) concluded that crystal fractionation is responsible for the mineral compositional variations, as we have shown above, but did not recognize the significant influence of Cr and Al on Na, Ti and other elements in the crystallizing cpx during MORB melt evolution. [Dick et al. \(2002\)](#) and [Thy \(2003\)](#) agree that the gabbros of Hole 735B and 1105A represent products of complex crystal mush zone (vs. “large” steady-state fully convective magma chamber) processes of multiple melt injections.

We should also emphasize that cpx crystals with  $\text{Mg}_{\text{Cpx}}^{\#} < 0.75$  are crystallized from variably evolved MORB melt of  $\text{Mg}_{\text{Melt}}^{\#} < 0.40$  (Fig. 7), which is parental to oxide gabbro, gabbro-norite, norite and the more evolved felsic lithologies. Consequently,  $\text{TiO}_2$  depletion in these cpx crystals (Fig. 4) is consistent with  $\text{TiO}_2$  depletion in the melt as a result of Ti–Fe oxide crystallization (Figs. 6 and 7).  $\text{Na}_2\text{O}$  depletion or flattening in these cpx crystals is consistent with Na-rich plagioclase crystallization in highly evolved silicic melt. Hence, there is no need to invoke complex magma chamber processes such as *in situ* boundary layer crystallization to explain these observations.

## 6. Summary

The apparently complex  $\text{TiO}_2$  and  $\text{Na}_2\text{O}$  variations in cpx from gabbroic lithologies in the lower oceanic crust are straightforward consequences of fractional crystallization-dominated MORB melt evolution and liquidus mineral stoichiometry control. The  $\text{TiO}_2$  and  $\text{Na}_2\text{O}$  maxima in cpx occur at  $\text{Mg}_{\text{Cpx}}^{\#} = \sim 0.76\text{--}0.73$ , which corresponds to  $\text{Mg}_{\text{Melt}}^{\#} = \sim 0.41\text{--}0.37$ . This in turns corresponds to liquidus temperature of  $\sim 1100 \pm 10$  °C, at which Fe–Ti oxides begin to crystallize. Because Ti and Cr both reside on M1 site of cpx and because Cr is highly compatible in cpx, Cr decreases whereas Ti increases complementarily with decreasing  $\text{Mg}_{\text{Cpx}}^{\#}$  for primitive cpx with  $\text{Mg}_{\text{Cpx}}^{\#} > 0.76$ . This is further manifested by the fact that  $\text{TiO}_2$  reaches its maximum when Cr approaches complete depletion at

$\text{Mg}_{\text{Cpx}}^{\#} = \sim 0.76\text{--}0.74$  in cpx. The  $\text{TiO}_2$  decrease with decreasing  $\text{Mg}_{\text{Cpx}}^{\#}$  at  $\text{Mg}_{\text{Cpx}}^{\#} < 0.74$  results from  $\text{TiO}_2$  depletion in the residual melt as a result of Fe–Ti oxide crystallization.

The  $\text{Na}_2\text{O}$  increase with decreasing  $\text{Mg}_{\text{Cpx}}^{\#}$  in cpx at  $\text{Mg}_{\text{Cpx}}^{\#} > 0.76$  is consistent with  $\text{Na}_2\text{O}$  increase with decreasing  $\text{Mg}_{\text{Melt}}^{\#}$  in the melt. At  $\text{Mg}_{\text{Melt}}^{\#} \leq 0.40$ ,  $\text{Na}_2\text{O}$  is sufficiently high whereas CaO and  $\text{Al}_2\text{O}_3$  are sufficiently low in the residual melt. This, plus the fact that  $\text{SiO}_2$  becomes sufficiently high in the melt as a result of Fe–Ti crystallization/removal, facilitates crystallization of Na-rich plagioclase, making  $\text{Na}_2\text{O}$  less available in the melt for cpx and explaining the reduced  $\text{Na}_2\text{O}$  abundance in cpx with  $\text{Mg}_{\text{Cpx}}^{\#} < 0.74$ . We emphasize further that low  $\text{Al}_2\text{O}_3$  and  $\text{TiO}_2$  cpx crystals with  $\text{Mg}_{\text{Cpx}}^{\#} < 0.75$  are not liquidus crystals of basaltic melt, but are in equilibrium with highly evolved felsic melts. Felsic vein lithologies with Na-rich plagioclase are volumetrically small but widespread in Hole 735B ([Niu et al., 2002a](#)). We anticipate that the compositional systematics of cpx from Hole 735B to be characteristic of cpx in all tholeiitic magmatic systems.

There is no need to invoke the *in situ* boundary layer crystallization model that is theoretically interesting, but practically unlikely because reduced extent of mantle melting and infrequent melt supply beneath slow-spreading ridges do not favour the development of steady-state and fully convective magma chambers.

## Acknowledgements

Discussion with all Leg 176 shipboard scientists has been very beneficial. S.S. would like to thank Johnathan Larco as well as her family for their support, advice and patience during her MSC research. Y.N. thanks the Leverhulme Trust for a Research Fellowship. We thank Laurence Coogan for discussion, and Bruno Scaillet, Wolfgang Bach and Lionel Wilson (Editor) for constructive comments that have helped improve the paper.

## References

- Annen, C., Scaillet, B., Sparks, R.S.J., 2006. Thermal constraints on the emplacement rate of a large intrusive complex: the Manaslu leucogranite, Nepal Himalaya. *Journal of Petrology* 47, 71–95.
- Bach, W., Alt, J.C., Niu, Y.L., Humphris, S.E., Erzinger, J., Dick, H.J.B., 2001. The chemical consequences of late-stage hydrothermal circulation in an uplifted block of lower ocean crust at the Southwest Indian Ridge: results from ODP Hole 735B (Leg 176). *Geochimica et Cosmochimica Acta* 65, 3267–3287.
- Batiza, R., Niu, Y.L., 1992. Petrology and magma chamber processes at the East Pacific Rise  $\sim 9^{\circ}30'N$ . *Journal of Geophysical Research* 97, 6779–6797.
- Batiza, R., Smith, T.L., Niu, Y.L., 1989. Geologic and petrologic evolution of seamounts near the EPR based on submersible and camera study. *Marine Geophysical Research* 11, 169–236.
- Batiza, R., Niu, Y.L., Zayac, W.C., 1990. Chemistry of seamounts near the East Pacific Rise: implications for the geometry of subaxial mantle flow. *Geology* 18, 1122–1125.
- Bloomer, S.H., Natland, J.H., Fisher, R.L., 1989. Mineral relationships in gabbroic rocks from fracture zones of Indian Ocean ridges: evidence for extensive fractionation, parental diversity and boundary-layer recrystallization. In: Saunders, A.D., Norry, M.J. (Eds.), *Magmatism in the Ocean Basins*, vol. 42. Geological Society Special Publication 107–124 pp.
- Cameron, M., Papike, J.J., 1980. Crystal chemistry of silicate pyroxenes. *Reviews in Mineralogy and Geochemistry* 7, 5–92.
- Casey, J.F., Karson, J.A., 1981. Magma chamber profiles from the Bay of Islands ophiolite complex. *Nature* 292, 295–301.
- Casey, J.F., Debleena, B., Zarian, P., 2007. Leg 179 synthesis: geochemistry, stratigraphy, and structure of gabbroic rocks drilled in ODP Hole 1105A, Southwest Indian Ridge. In: Casey, J.F., Miller, D.J. (Eds.), *Proceedings of ODP. In: Scientific Results 179. (Ocean Drilling Program)*, College Station, TX, pp. 1–125. doi:10.2971/odp.proc.sr.189.001.2007.
- Christie, D.M., Carmichael, I.S.E., Langmuir, C.H., 1986. Oxidation states of mid-ocean ridge basalt glasses. *Earth and Planetary Science Letters* 79, 397–411.
- Coogan, L.A., 2007. The lower oceanic crust. In: Turekian, K., Holland, H.D. (Eds.), *Treatise on Geochemistry*. Elsevier.
- Coogan, L.A., Kempton, P.D., Saunders, A.D., Norry, M.J., 2000. Melt aggregation within the crust beneath the Mid-Atlantic Ridge: evidence from plagioclase and clinopyroxene major and trace element compositions. *Earth Planetary Science Letters* 176, 245–257.
- Danyushevsky, L.V., 1998. The effect of small amount of H<sub>2</sub>O on fractionation of mid-ocean ridge magmas. *Eos, Transaction of American Geophysical Union* 79, 375.
- Dick, H., Natland, J., ODP Leg 176 Shipboard Party, 2000. A long in-situ section of the lower ocean crust: results of ODP Leg 176 drilling at the Southwest Indian Ridge. *Earth and Planetary Science Letters* 179, 31–51.

- Dick, H.J.B., Schouten, H., Meyer, P.S., Gallo, D.G., Bergh, H., Tyce, R., Patriat, P., Johnson, K.T.M., Snow, J., Fisher, A., 1991. Tectonic evolution of the Atlantis II Fracture Zone. In: Von Herzen, R.P., Robinson, P.T., et al. (Eds.), *Proc. ODP. In: Sci. Results*, vol. 118. Ocean Drilling Program, College Station, TX, pp. 359–398.
- Dick, H.J.B., Natland, J.H., Miller, D.J., et al. 1999. Proceedings of ODP, Initial Report, 176 [CDROM]. Available from: Ocean Drilling Program, Texas A&M University, College Station, TX 77845-9547, U.S.A.
- Dick, H.J.B., Ozawa, K., Meyer, P.S., Niu, Y., Robinson, P.T., Constantin, M., Herbert, R., Natland, J., Hirth, G., Mackie, S., 2002. Primary silicate mineral chemistry of a 1.5-km section of very-slow spread lower ocean crust: ODP Hole 735B, Southwest Indian Ridge. In: Natland, J.H., Dick, H.J.B., Miller, D.J., Von Herzen, R.P. (Eds.), *Proceedings of ODP Scientific Results*, vol. 176 1–60 pp.
- Elthon, D., Stewart, M., Ross, D.K., 1992. Compositional trends of minerals in oceanic cumulates. *Journal of Geophysical Research* 97, 15189–15199.
- Grove, T.L., Kinzler, R.J., Bryan, W.B., 1992. Fractionation of mid-ocean ridge basalt (MORB). In: Phipps Morgan, J., Blackman, D.K., Sinton, J.M. (Eds.), *Mantle flow and melt generation at mid-ocean ridges: American Geophysical Union Monograph*, vol. 71, pp. 281–310.
- Hart, S.R., Dunn, T., 1993. Experimental cpx/melt partitioning of 24 trace elements. *Contributions to Mineralogy and Petrology* 113, 1–8.
- Kelemen, P.B., Koga, K., Shimizu, N., 1997. Geochemistry of gabbro sills in the crust/mantle transition zone of the Oman ophiolite: implications for the origin of the lower oceanic crust. *Earth and Planetary Science Letters* 146, 475–488.
- Korenaga, J., Kelemen, P.B., 1998. Melt migration through the oceanic lower crust: a constraint from melt percolation modeling with finite solid diffusion. *Earth and Planetary Science Letters* 156, 1–11.
- Langmuir, C.H., 1989. Geochemical consequences of in situ crystallization. *Nature* 340, 199–205.
- Langmuir, C.H., Klein, E.M., Plank, T., 1992. Petrological systematics of mid-ocean ridge basalts: constraints on melt generation beneath ocean ridges. In: Phipps Morgan, J., Blackman, D.K., Sinton, J.M. (Eds.), *Mantle flow and melt generation at mid-ocean ridges: American Geophysical Union Monograph*, vol. 71, pp. 183–280.
- MacLeod, C.J., Yaouancq, G., 2000. A fossil melt lens in the Oman ophiolite: implications for magma chamber processes at fast spreading ridges. *Earth and Planetary Science Letters* 176, 357–373.
- McBirney, A.R., Noyes, R.M., 1979. Crystallization and layering of the Skaergaard intrusion. *Journal of Petrology* 20, 487–554.
- Morimoto, N., 1988. Nomenclature of pyroxene. *Mineralogical Magazine* 52, 535–550.
- Natland, J.H., 1980. Effect of axial magma chambers beneath spreading centers on the composition of basaltic rocks. Initial Report: Deep Sea Drilling Project, vol. 54 833–850 pp.
- Natland, J.H., Dick, H.J.B., 2001. Formation of the lower ocean crust and the crystallization of gabbroic cumulates at a very slowly spreading ridge. *Journal of Volcanology and Geothermal Research* 110, 191–233.
- Natland, J.H., Dick, H.J.B., 2002. Stratigraphy and composition of gabbros drilled at Ocean Drilling Program Hole 735B, Southwest Indian Ridge: a synthesis of geochemical data. In: Natland, J.H., Dick, H.J.B., Miller, D.J., Von Herzen, R.P. (Eds.), *Proceedings of ODP. In: Scientific Results*, vol. 176. Ocean Drilling Program, College Station, TX 1–69 pp.
- Nielsen, R.L., Delong, S.E., 1992. A numerical approach to boundary layer fractionation: application to differentiation in natural magma systems. *Contributions to Mineralogy and Petrology* 110, 355–369.
- Niu, Y.L., 1997. Mantle melting and melt extraction processes beneath ocean ridges: evidence from abyssal peridotites. *Journal of Petrology* 38, 1047–1074.
- Niu, Y.L., 2004. Bulk-rock major and trace element compositions of abyssal peridotites: implications for mantle melting melt extraction and post-melting processes beneath ocean ridges. *Journal of Petrology* 45, 2423–2458.
- Niu, Y.L., 2005. Generation and evolution of basaltic magmas: some basic concepts and a hypothesis for the origin of the Mesozoic–Cenozoic volcanism in eastern China. *Geological Journal of China Universities* 11, 9–46.
- Niu, Y.L., Batiza, R., 1997. Trace element evidence from seamounts for recycled oceanic crust in the eastern equatorial Pacific mantle. *Earth and Planetary Science Letters* 148, 471–484.
- Niu, Y.L., Hékinian, R., 1997a. Spreading rate dependence of the extent of mantle melting beneath ocean ridges. *Nature* 385, 326–329.
- Niu, Y.L., Hékinian, R., 1997b. Basaltic liquids and harzburgitic residues in the Garrett Transform: a case study at fast-spreading ridges. *Earth and Planetary Science Letters* 146, 243–258.
- Niu, Y.L., O'Hara, M.J., 2008. Global correlations of ocean ridge basalt chemistry with axial depth: a new perspective. *Journal of Petrology* 49, 633–664.
- Niu, Y.L., Collerson, K.D., Batiza, R., Wendt, I., Regelous, M., 1999. The origin of E-type MORB at ridges far from mantle plumes: the East Pacific Rise at 11°20'N. *Journal of Geophysical Research* 104, 7067–7087.
- Niu, Y.L., Gilmore, T., Mackie, S., Greig, A., Bach, W., 2002a. Mineral chemistry, whole-rock compositions and petrogenesis of ODP Leg 176 gabbros: data and discussion. In: Natland, J.H., Dick, H.J.B., Miller, D.J., Von Herzen, R.P. (Eds.), *Proc. ODP: Sci. Results*, vol. 176 1–60 pp.
- Niu, Y.L., Regelous, M., Wendt, J.I., Batiza, R., O'Hara, M.J., 2002b. Geochemistry of near-EPR seamounts: importance of source vs. process and the origin of enriched mantle component. *Earth and Planetary Science Letters* 199, 327–345.
- Niu, Y.L., Waggoner, G., Sinton, J.M., Mahoney, J.J., 1996. Mantle source heterogeneity and melting processes beneath seafloor spreading centers: the East Pacific Rise 18°–19°S. *Journal of Geophysical Research* 101, 27711–27733.
- O'Hara, M.J., 1968. Are ocean floor basalts primary magmas? *Nature* 220, 683–686.
- O'Hara, M.J., 1977. Geochemical evolution during fractional crystallization of a periodically refilled magma chamber. *Nature* 266, 503–507.
- O'Hara, M.J., Mathews, R.E., 1981. Geochemical evolution in an advancing, periodically replenished, periodically tapped, continuously fractionating magma chamber. *Journal of Geological Society of London* 138, 237–277.
- Regelous, M., Niu, Y.L., Wendt, J.I., Batiza, R., Greig, A., Collerson, K.D., 1999. An 800 Ka record of the geochemistry of magmatism on the East Pacific Rise at 10°30'N: insights into magma chamber processes beneath a fast-spreading ocean ridge. *Earth and Planetary Science Letters* 168, 45–63.
- Robinson, P.T., Von Herzen, R., et al., 1989. *Proc. ODP. Init. Repts.*, vol. 118. Ocean Drilling Program, College Station, TX.
- Roeder, P.L., Emslie, R.F., 1970. Olivine-liquid equilibrium. *Contributions to Mineralogy and Petrology* 29, 275–289.
- Singh, S.C., Crawford, W.C., Carton, H., Seher, T., Combier, V., Cannat, M., Canales, J.P., Dusunur, D., Escartin, J., Miranda, J.M., 2006. Discovery of a magma chamber and faults beneath a Mid-Atlantic Ridge hydrothermal field. *Nature* 442, 1029–1032.
- Sinha, M.C., Navin, D.A., MacGregor, L.M., Constable, S., Pierce, C., White, A., Heinson, G., Inglis, M.A., 1997. Evidence for accumulated melt beneath the slow-spreading Mid-Atlantic Ridge. *Philosophical Transaction of the Royal Society of London*, A 355, 233–253.
- Sinton, J.M., Detrick, R.S., 1992. Mid-ocean ridge magma chambers. *Journal of Geophysical Research* 97, 197–216.
- Stolper, E., 1980. A phase diagram for mid-ocean ridge basalts: preliminary results and implications for petrogenesis. *Contributions to Mineralogy and Petrology* 74, 13–27.
- Thy, P., 2003. Igneous petrology of gabbros from Hole 1105A: oceanic magma chamber processes. In: Casey, J.F., Miller, D.J. (Eds.), *Proceedings of ODP: Scientific Results*, vol. 179 1–76 pp.
- Walker, D., Shibata, T., DeLong, S.E., 1979. Abyssal tholeiites from the Oceanographer Fracture Zone, II. Phase equilibria and mixing. *Contribution to Mineralogy and Petrology* 70, 111–125.
- Weaver, J.S., Langmuir, C.H., 1990. Calculation of phase equilibrium in mineral melt systems. *Computers and Geosciences* 16, 1–19.